# CHAPTER 6
# SPATIO-TEMPORAL PATTERNS OF AEROSOL BASED ON SATELLITE OBSERVATORY

## 6.1 Introduction

The physical, optical and radiative properties of dust aerosols are of great importance over the globe, especially over the desert areas and regions affected by frequent and intense dust outflows, for the attenuation of solar radiation, mixing processes in the atmosphere, interaction between dust aerosols and clouds and thermal heating of the troposphere (e.g. Rosenfeld *et al*., 2001; Dey *et al*., 2004; Prasad *et al*., 2009; Gautam *et al*., 2009a; Anton *et al*., 2011; Christopher *et al*., 2011). The characterization of aerosol optical and microphysical properties is crucial to the understanding of their effect on the Earth-atmosphere radiation budget and climate (e.g. Haywood *et al*., 1999; Meloni *et al*., 2005; Marey *et al*., 2011). Thus, it is necessary to analyze the seasonality of dust aerosols, particularly over regions with frequent and intense dust storm events, which affects solar radiation, ecosystems and human health (Singh *et al*., 2008; Nastos *et al*., 2010; Maghrabi *et al*., 2011). Assessment of the aerosol properties is necessary for understanding the aerosol radiative effects on climate using remote sensing techniques and in-situ measurements. Furthermore, changes in the vertical structure of the atmospheric aerosols due to formation of distinct aerosol layers aloft may significantly alter the radiative forcing in to the atmosphere (Guan *et al*., 2010; Lemaître *et al*., 2010). These elevated aerosol layers mainly consist of dust plumes transported thousands of kilometers away from their sources causing severe affects on air quality and public health (e.g. Torres *et al*., 2002; Marey *et al*., 2011; Rashki *et al*., 2012).

Atmospheric aerosols affect the incoming and outgoing solar radiation directly by scattering and absorbing the solar and terrestrial radiation and indirectly by modifying the physical and radiative properties of clouds (Charlson *et al*., 1992; Rosenfeld *et al*., 2008). AOD is one of the most important optical properties of aerosols, which is directly related to the magnitude of attenuation of direct solar radiation by scattering and absorption

processes. Assessment of the aerosol properties is necessary for understanding the aerosol radiative effects on climate and retrieving the aerosol optical properties using remote-sensing techniques. Changes in the atmospheric aerosol load and land surface properties alter the energy balance of earth's atmosphere (Wild *et al*., 2012).

Satellite monitoring of aerosols over the desert areas and downwind regions over the globe has been increasingly available via observations of Total Ozone Mapping Spectrometer (TOMS) and Ozone Monitoring Instrument (OMI) (e.g. Hsu *et al*., 1999; Alpert *et al*., 2004; Engelstaedter *et al*., 2006; Kaskaoutis *et al*., 2010), Moderate Resolution Imaging Spectroradiometer (MODIS) Deep Blue algorithm (e.g. Hsu *et al*., 2004; Gautam et al., 2011), Multi-angle Imaging Spectro-Radiometer (MISR) (Kalashnikova *et al*., 2005; Kahn *et al*., 2009), SEVIRI (e.g. Bou Karam *et al*., 2010; Haywood *et al*., 2011) and Cloud-Aerosol Lidar and Infrared Pathfinder Satellite Observation (CALIPSO) (e.g. Generoso *et al*., 2008; Liu *et al*., 2008a, b). Individual ground-based observations represent point measurements and do not have coverage required to map regional or global distributions of aerosols. Thus, satellite remote sensing has made tremendous progress within the last 10-15 years; recently, MODIS (Chu et al., 2003; Wang and Christopher, 2003), MISR (Liu et al., 2007). Despite the larger uncertainties compared to ground-based observations, satellite remote sensing allows the spatial distribution and properties of aerosols to be assessed, and it also has the major benefit of allowing complete and synoptic mapping of a large area in a single snapshot (Kosmopoulos *et al*., 2008).

This Chapter focuses on dust-aerosol monitoring over the arid environment of Sistan and surroundings mainly aiming to present the first climatology of dust-aerosol patterns, i.e. multi-year, seasonal and monthly variations of spatial and vertical extend of aerosols by means of multiple satellite observations. A large database of remotely sensed aerosol loading have been compiled in order to analyze its spatio-temporal variability, and how this load interacts with different variables that characterize the dynamic and thermodynamic states of the environment. More specifically, the TOMS-AI and OMI-AI values are utilized along with AOD retrievals from MODIS Deep Blue algorithm and MISR over desert regions. The diversity of this database relies on the different satellite product retrieval techniques and calibration procedures that provide a synergistic approach to complement the analysis.

## 6.2 Satellite data sets

Aerosol datasets used in this Chapter correspond to TOMS-Nimbus 7(N7T, 1978-1992), TOMS-Earth Probe (EP, 1996-2005), Aura-OMI (2005-2011), Terra-MISR (2000-2010), Aqua-MODIS (2002-2011) and Terra-MODIS (2000-2010) (Table 6.1). For all the above-mentioned sensors the AI and AOD values are analyzed over Sistan and surrounding regions both temporally and spatially in order to reveal the annual variability as well as the trend in aerosol loading during the different periods. It should be noted that it's the first time that aerosols are systematically monitored over the region via satellite remote sensing. Although, TOMS-Earth Probe AI data are available till 2005 due to calibration issues associated with sensor degradation, trend analysis of the data after 2001 is not recommended as per the NASA TOMS science team and other available documentation (Kiss *et al*., 2007; Gautam *et al*., 2009). Hence, we restrict the trend analysis of AI data till 2001. In the following, each sensor used for aerosol retrievals over the region is described.

**Table 6.1:** Satellite datasets used in this thesis

| Satellite sensor | Period | Product | Spectral resolution | Spectral band |
|---|---|---|---|---|
| TOMS Nimbus-7 | 11/1978- 4/1992 | AI Daily level-2 | 1.25° x 1° | UV |
| Earth Probe | 8/1997- 12/2001 | AI Daily level-2 | 1.25° x 1° | UV |
| OMI | 01/2005- 12/2011 | AI Daily level-2 | 0.25° x 0.25° | UV |
| MISR Terra | 3/2000- 12/2010 | AOD Daily level-3 | $0.5^{o}$ x 0.5° | 558 nm |
| Aqua-MODIS **(Deep Blue)** | 08/2002- 12/2011 | AOD Daily level-3 | $1^{o}$ x $1^{o}$ | 550 nm |
| Terra-MODIS **(Deep Blue)** | 03/2000- 12/2007 | AOD Daily level-3 | $1^{o}$x$1^{o}$ | 550 nm |

### 6.2.1 TOMS, OMI sensors

The TOMS Aerosol Index (AI) is the longest available aerosol database on board several satellites (Nimbus-7, Meteor-3, Earth Probe, Aura) from 1978 to present. For about four decades, the TOMS sensors have been providing useful global data on the long-range transport of dust plumes (McPeters *et al*, 1996, Griffi *et al*, 2001; Badarinath *et al*., 2010). TOMS was designed to provide global estimates of total ozone column using

backscattered UV radiance measured at six bands (313, 318, 331, 340, 360 and 380 nm). Aerosol measurements are made in the three longest wavelengths, where gaseous absorption is weak and where the backscattered radiation is primarily controlled by molecular and aerosol scattering, surface reflection and scattering by clouds.

OMI is on board the Finnish–Dutch Aura satellite launched in July 2004. OMI was designed to replace TOMS to continue recording total ozone and other atmospheric parameters related to ozone chemistry and climate. OMI has a spatial resolution of 13 × 24 km at nadir and uses the same retrieval algorithm as TOMS (Torres *et al.*, 1998). It measures back scattered radiances in the near UV region, and using these measurements, the retrieval algorithm computes an absorbing AI, which is a qualitative measure of the presence of UV-absorbing aerosols over all terrestrial surfaces, including deserts and snow-ice covered areas.

The AI has been established as a powerful tool in determining the sources of dust aerosols (Prospero *et al.*, 2002; Alpert *et al.*, 2004; Engelstaedter *et al.*, 2006). The AI is a measure of the wavelength-dependent change in Rayleigh-scattered irradiance from aerosol absorption and is especially suitable for detecting the presence of UV-absorbing aerosols (desert dust, soot, volcanic ash) above high reflecting surfaces, such as deserts and snow/ice areas. These aerosol types are also detected intermingled with clouds and above cloud decks. This is the great advantage between AI and AOD derived from other satellite sensors, like MODIS. The AI can differentiate very well the absorbing and non-absorbing aerosols, by providing a measure of absorption of the UV radiation by smoke and desert dust. The absorbing AI is defined as the difference between the measured (includes aerosol effects) spectral contrast at the 360 nm and 331nm wavelength radiances and the contrast calculated from the radiative transfer theory for a pure molecular (Rayleigh) atmosphere (Ahmad *et al.*, 2003). AI is mathematically defined as:

$$AI = -100[\log_{10}(I_{360}/I_{331})_{meas} - \log_{10}(I_{360}/I_{331})_{calc}] \quad (6.1)$$

where I is the radiance. Since $I_{360}$ calculation uses reflectivity derived from the $I_{331}$ measurements, the AI definition essentially simplifies to:

$$AI = 100 \log_{10} (I_{360\_meas}/I_{360\_calc}) \quad (6.2)$$

The method for the AI retrievals via Eq. (6.1) is based on the principle that for a fixed 360-nm radiance the $I_{331}/I_{360}$ spectral contrast is larger for non-absorbing aerosols and clouds and decreases with increasing absorption. Thus, UV-absorbing aerosols (e.g. dust, smoke and volcanic ash) produce smaller contrast than predicted by the pure Rayleigh scattering atmospheric model; consequently they yield positive values. On the other hand, the non-absorbing aerosols (e.g. sea-salt and sulfate particles from both natural and anthropogenic sources) produce greater contrast and negative values (Torres *et al.*, 1998; Kaskaoutis *et al.*, 2010c). Nevertheless, negative AI values can also be caused by features other than non-absorbing aerosols. Amongst these features are elevated clouds and spectral slopes in the surface albedo between the two wavelengths used for the AI detection. Moreover AI<0 indicates absence of elevated absorbing aerosols, since the AI increases with altitude for the same aerosol load (Prospero *et al.*, 2002). This is the main disadvantage in the AI use as a measure of the aerosol load in the atmosphere. Nevertheless, desert dust has a direct effect on AI because of its strong dependence on the imagery part of the refractive index in the UV wavelengths (Sinyuk *et al.*, 2003; De Graaf et al., 2005), and due to the fact that it is usually transported at elevated layers into the atmosphere. On the other hand, the presence of clouds results in near-zero values for the AI (Hsu *et al.*, 1999).

In interpreting the results, care has to be taken that some surface effects, such as sea glint and ocean color, can also enhance the AI. The advantage of the AI is that it can be applied over both oceans and land, thus improving the knowledge about the distribution of dust sources and transport pathways over the globe (Middleton and Goudie, 2001; Israelevich *et al.*, 2002; Prospero *et al.*, 2002; Alpert *et al.*, 2004). However, there are several factors that complicate the interpretation of the TOMS and OMI AI values. The detection of absorbing aerosols is based on the perturbation of the backscattered UV flux that originates below the aerosol layer. Because the albedo of land and water surfaces in the UV is typically low (Herman and Celarier, 1997), essentially all of the UV upwelling flux originates from backscatter from the gaseous constituents in the atmosphere. Consequently, for any given total column aerosol concentration, aerosol at the top of the atmosphere will yield a larger value of AI than an equal amount of aerosol at a lower altitude. Hsu *et al.* (1999) showed that the altitude dependence of aerosols is almost linear. Thus, TOMS and OMI sensors are more sensitive to aerosols in the middle and upper

troposphere and in the stratosphere; aerosols lofted to these altitudes are most likely to be carried over larger distances. On the other hand, both sensors are least sensitive to aerosols in the boundary layer, where aerosol residence times are short. In fact, aerosols below 500-1000 m are unlikely to be detected by TOMS and OMI (Torres *et al*., 1998; 2002; Kaskaoutis *et al*., 2012b). For these reasons, one cannot simply use the AI values to compare the relative strengths of dust sources in different climate and meteorological regimes. Nonetheless, within specific regions and in specific seasons, the AI should provide a rough measure of relative dust concentrations and, hence, relative source strength. Moreover, TOMS and OMI can retrieve AI in partially clouded pixels, but not in regions covered with clouds except for aerosol above the cloud deck (Herman *et al*., 1997; Torres *et al*., 1998). Nevertheless, TOMS should yield relatively unbiased distributions over arid regions because of the sparse cloud cover. The discrimination between UV-absorbing and non-absorbing aerosols via satellites can find application in the identification of such particles as well as their source regions. Thus, the detection and mapping of dust events and dust transport pathways have benefited greatly from the use of remote sensing.

The TOMS-OMI data used in this Chapter is the most recently re-classified and re-calculated version (Version 8). The dataset is composed of an ensemble of daily records from three satellite mission retrievals namely: (1) Nimbus 7 (N7T, 1978-1993), (2) Earth Probe (EP, 1996-2005) and (3) OMI satellite (2004 to 2011). Periods of data from 2000 to 2005 for EP and 2008 to 2009 for OMI were removed from the AI records. Data was removed because EP present a calibration drift produced by sensor degradation affecting the retrieval (Kiss *et al*. 2007; Bollasina *et al*., 2008) and because OMI presents an obstruction in the sensors field of view causing stripes of bad data (see *http://macuv.gsfc.nasa.gov/*, 2010 for details). In addition, AI values less than 0.5 are treated as missing values because contamination of the variable by sea-glint and water-leaving radiances (Courier *et al*., 2008). The entire compilation of TOMS-OMI AI was obtained from the Giovanni website (*http://giovanni.gsfc.nasa.gov/*) covering the south west Asia bounded from 20 to 34$^{o}$N and 52 to 72$^{o}$E in a 1° x 1.25° spatial resolution for TOMS and 0.25$^{o}$x0.25$^{o}$ for OMI.

### 6.2.2 MODIS sensors

The MODIS sensors onboard NASA's Terra (launched in December 1999) and Aqua (launched in May 2002) satellites have been acquiring nearly daily global coverage data in 36 spectral bands from visible to thermal infrared (29 spectral bands with 1-km, 5 spectral bands with 500-m, and 2 spectral bands with 250-m, nadir pixel dimensions). The MODIS sensor is on board the polar-orbiting NASA-EOS Terra and Aqua spacecrafts with equator crossing times of 10:30 and 13:30 Local Solar Time, respectively (Levy *et al*., 2007). A nearly global image is produced due to the large swath widths of MODIS and instrument-scanning angle of 110° (Levy *et al*., 2003). Numerous parameters describing various properties over land and ocean surfaces as well as in the atmosphere are retrieved operationally from MODIS data at different spatial and temporal resolutions (daily, weekly and monthly). Aerosol retrievals from MODIS observations are performed over land and ocean surfaces by means of two separate algorithms described in literature (Kaufman and Tanrè, 1998). As discussed in validation studies (e.g. Chu *et al*., 2002; Remer *et al*., 2002) a different expected uncertainty is applied over ocean (±0.03±0.05AOD) and over land (±0.05±0.2AOD) for the previous Collection 4 (C004) retrievals. Over land, even larger errors can be found in coastal zones due to sub-pixel water contamination. Similarly, a significant watercolor contribution can reduce the ocean AOD retrieval quality in coastal areas. In dust aerosol regimes, the retrieved AOD values have greater error due to non-spherical effects (Remer *et al*., 2002; Chu *et al*. 2002; Levy *et al*., 2003).

The retrieval of AOD from MODIS sensor is done with three independent algorithms using seven of the sensor spectral bands between 0.47 and 2.130 µm that are sensitive to aerosol content in the atmospheric column. The first two algorithms are based on the "dark target" approach and were designed to retrieve AOD over ocean and non-bright land surfaces (Kaufman *et al*. 1997; Tanre *et al*. 1997). The latter, called "Deep Blue", is able to retrieve AOD over bright land surfaces (Hsu *et al*. 2004, 2006). Whereas TOMS and OMI AI is only capable of retrieving absorbing aerosols, MODIS AOD measurements are sensitive to both absorbing and non-absorbing aerosols. In addition, MODIS sensors are capable of providing additional and much more accurate aerosol properties (i.e., scattering angle, Angstrom exponent, etc) because it uses a multiple wavelength retrieval technique and cloud masking procedures (Remer *et al*., 2005). The aerosol properties are derived by

the inversion of the MODIS-observed reflectance using pre-computed radiative transfer tables based on aerosol models (Remer *et al*., 2005; Levy *et al*., 2007). The initial versions of the MODIS algorithms have been under continual development, and have recently received an improved aerosol determination, via processing to Collection 5 (C005) (Levy *et al*., 2007, 2010). In general, OMI-AI and MODIS-AOD are somewhat complementary; the first is ideal for initial dust detection and the second can be used to both identify plumes and sources at higher spatial resolution.

The "dark target" approach is unable to provide any aerosol retrievals above arid and desert surfaces, as in the Sistan region, due to high surface albedo, which is similar to the radiation reflected by the aerosol layers. Thus, only the "Deep Blue" algorithm is able to provide such aerosol retrievals over the region, which is used in the present analysis. An alternative method for the dust-plume identification as well as its source region and spatial extent is the land-surface temperature observations from the satellite sensors using the infrared channels. This method has become increasingly available in recent years and is assumed quite accurate, since the temperature variation between the dust plume and the underlying surface can be very large and easily detected by the satellite sensors. Two characteristic cases for the dust identification via the infrared satellite channels are presented in the following images (Fig. 6.1).

A heavy dust plume was observed over Sistan region, southern Afghanistan and northern Pakistan on June 14, 2004. The dust appears to be blowing out of the Sistan basin. In this MODIS image, the dust is masking the arid deserts of Afghanistan and Pakistan and is sweeping around the Chagai Hills, the dark land in the center of the storm. The crescent of the Siahan mountain range in Pakistan is preventing the dust from blowing further south. Once airborne, the dust cools considerably, which makes it stand out in this surface temperature image. The dust is about 40 $^{o}$C cooler than the ground-land temperature, which reaches up to 57 $^{o}$C in pockets where the land is darker, and therefore, absorbs more sunlight. Patches of clouds also show up as extremely cold blue regions in the temperature image. Though the dust is easy to be detected in the true color image, surface temperature images can make dust storms easier to be detected in cases when the dust plume has the same color with the ground.

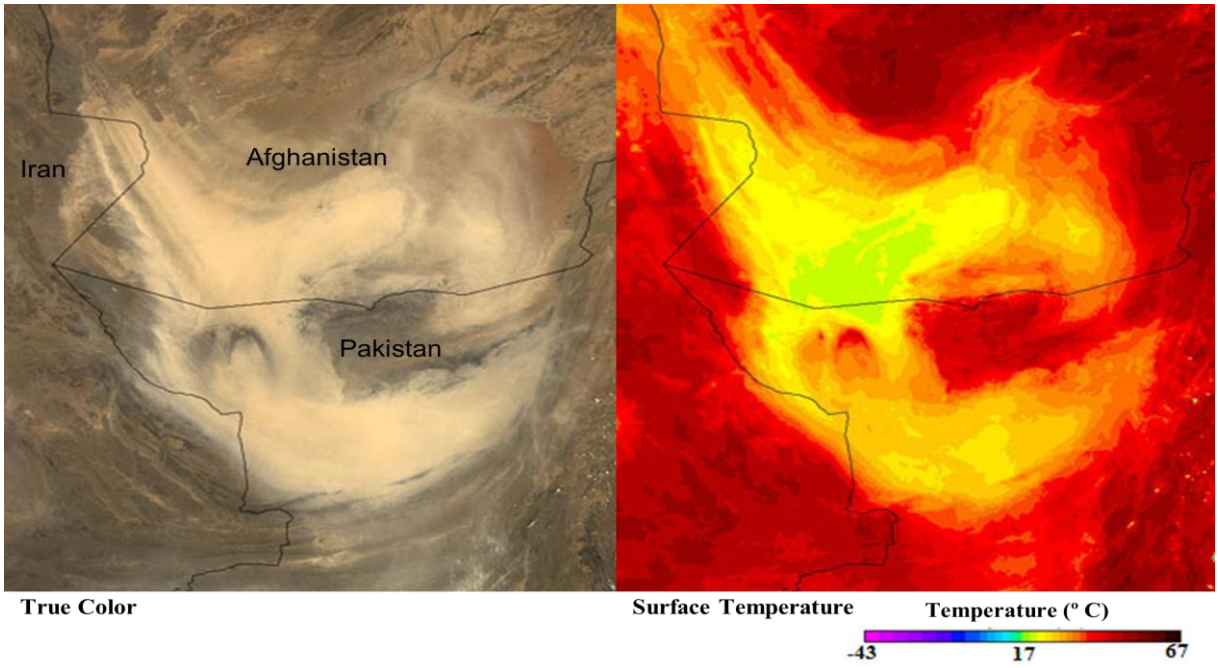


**Figure 6.1:** Terra-MODIS satellite true color and infrared (temperature) images captured on June 14, 2004 over Iran, Afghanistan and Pakistan.[Source*: http://earthobservatory.nasa.gov/IOTD/view.php?id=4574*]

In this analysis a set of MODIS data downloaded from the NASA Atmosphere Archive and Distribution System (LAADS, *http://ladsweb.nascom.nasa.gov/*) was used. Daily and monthly AOD data at 550 nm were obtained during the period July 2002 to December 2011 from the Aqua platform and from Terra platform in the period March 2000 to December 2010 by means of the Deep Blue algorithm. The data covers the section of south west Asia that includes the Sistan region at an equal-angle latitude-longitude grid with a horizontal resolution of 1° x 1°.

### 6.2.3 Multi-angle Imaging SpectroRadiometer (MISR) sensor

The Multi-angle Imaging SpectroRadiometer (MISR) was launched into polar Earth orbit aboard NASA's Terra satellite on December 18, 1999. The instrument contains 9 push broom cameras pointed at nadir and along-track view angles of 70.5º, 60º, 46.1º, 26.1º forward and backward of nadir, with spectral bands at 446, 558, 672, and 866 nm. Surface and atmospheric targets within the observed swath (~400 km) are viewed at all 9 angles over a span of 7 minutes with an intrinsic spatial resolution of 275 m. No instrument that combines MISR's attributes—multi angle imaging at moderately high spatial resolution with near-simultaneous temporal sampling; stable and accurate on-board

calibration suitable for climate quality science; and global coverage had not flown in space prior to Terra launch, nor is there is a similar capability currently available on any other satellite platform (Kahn *et al*. 2009; Diner *et al*., 2010). Due to multi-angle viewing MISR is able to obtain aerosol retrievals over desert and arid surfaces of high reflectance.

Thus, additionally to MODIS and OMI, AOD data was retrieved from the MISR sensor mounted on the EOS-Terra satellite to complement the analysis. The aerosol retrievals are based on prescribed tables of forward radioactive calculations that are then compared with the MISR observations to determine AOD and other properties (Diner *et al*. 1998). While MODIS provides information on aerosol concentrations with approximately 1-2 day global coverage, MISR repeats coverage every 7 to 9 days due to the much smaller swath (~400 km against ~2300 km). This lengthy cycle limits the use of MISR data for high temporal analysis, but the high accuracy of the retrieved data over bright deserts provides the necessary additional synergistic information to supplement the study. The MISR AOD dataset is obtained from Giovanni website (*http://giovanni.gsfc.nasa.gov//)* over southwest Asia containing Sistan region at a 0.5° x 0.5° spatial resolution from February 2000 to December 2010.

**6.2.4 Giovanni data base**

From Giovanni online data visualization tool one can easily obtain several atmospheric, hydrological, land and surface variables by selecting the desired variables via the satellite sensors or via models and re-analysis on a global scale. The user has the ability to select the study region by inserting in the system the geographical coordinates (Lat, Long) as well as the study period. The user may have the data as lat-long maps, as dataseries, as scatter plots, etc… There is also the possibility to download the dataset in different formats (ASCII files) and then to analyze them through statistical software. Giovanni online visualization tool has been increasingly available during the last years, mainly due to its simplicity to provide accurate satellite datasets for specific regions and periods. However, it cannot provide observations of high resolution, i.e. MODIS Level 2 retrievals (10 x 10 km) or the original Level 1 satellite observations.

### 6.3. Multi-year variation of aerosol properties over Sistan

This section analyzes the multi-year fluctuation of the aerosol properties, AOD and AI, over Sistan region as obtained from satellite observations. In addition, the satellite observations, although some of them correspond to different periods, are compared to each other and the trend in aerosols is examined via linear regression analysis in order to reveal the tendency in aerosol loading over Sistan region. The AI and AOD time series from the multiple satellite sensors are shown in Fig. 6.2, while the lower panel concentrates on the 2000s. In general, the results show considerable inter-annual and intra-seasonal variability for all aerosol characteristics, revealing a pronounced seasonally-dependent aerosol field over Sistan.

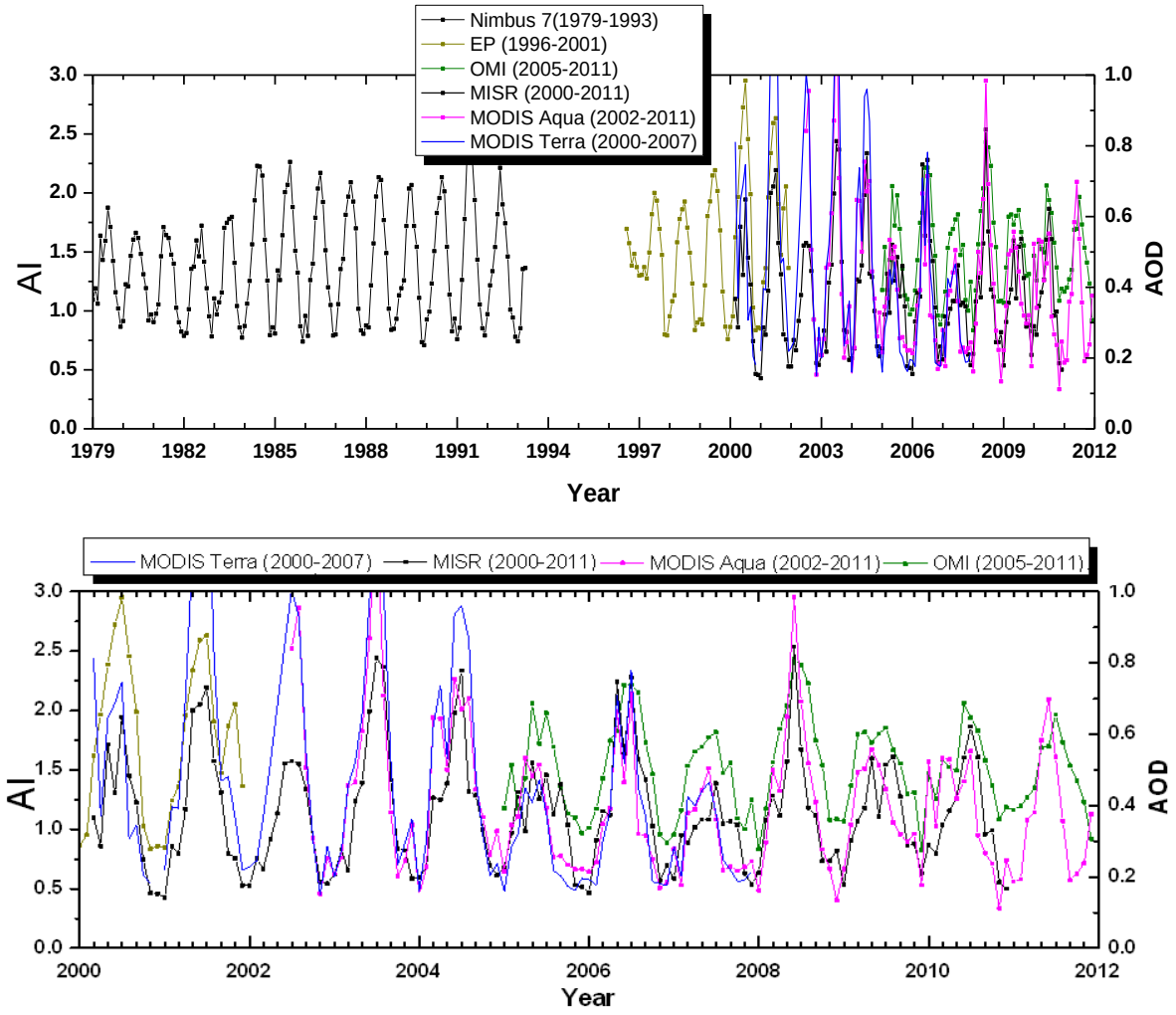


**Figure 6.2:** Data series of Aerosol Index (AI) values from Nimbus 7, Earth Probe and Ozone Monitoring Instrument (OMI), as well as aerosol optical depth (AOD) values from MISR and Terra/Aqua-MODIS over Sistan region.

Dust outbreaks originating from the Hamoun Basin during summer provide the necessary amount of aerosols in order to enhance the AI and AOD values at levels above ~2.0 and ~0.7, respectively on monthly basis, which are considered very high and characteristic of desert environments (Kim *et al*., 2011; Marey *et al*., 2011). Figure 6.2 shows enhanced AI values from Nimbus 7 after 2004 compared to the previous years, while both AOD and AI values are very high during early 2000s, especially in 2001. The large increase in AOD during 2000-2003 is mainly defined at the summer maximum values, while the winter ones are nearly similar for all years.

The AI and AOD data series during the common periods, i.e. after 2000, show a similar monthly and yearly variation for all sensors. Their relationships show significant correlation between Terra and Aqua MODIS AODs ($R^2$=0.96), as well as between MISR and Terra MODIS ($R^2$=0.79) and MISR vs Aqua-MODIS ($R^2$=0.79). This suggests that the satellite sensors reveal similar aerosol load and variability over Sistan giving credit to the present results, which, however, need comparison and extra validation with ground-based instrumentation, i.e. sun photometers, which, however, are lacking over Sistan region. The correlation coefficients from the comparison between the monthly values of AOD and AI from the different sensors are summarized in Table 6.2. The results show that all the correlations are statistically significant at 95% confidence level.

This research is the first that examines the aerosol variations and trends over Sistan region by means of multiple satellite platforms in the absence of long-term ground-based data series. Previous studies examining aerosol variations and trends over southwest Asia have been conducted by Yoon *et al*. (2011) for selected AERONET locations in the Middle East, by Dey and di Girolamo (2011) and Kaskaoutis *et al*. (2011) over the Indian sub-continent and adjoining oceanic region using MISR and MODIS data, respectively during the last decade. These studies agree that there is a general increase in aerosol loading over southwest Asia, which is mainly attributed to significant increase in anthropogenic emissions. In contrast, aerosols over the Sistan region are mainly composed of soil and dust particles, whereas the anthropogenic component is rather low due to absence of major industries and urban centers over the region. Note also that southeastern Iran, southern Afghanistan and western Pakistan are very sparsely populated areas. Thus, the variability in aerosol emissions and atmospheric lifetime is strongly influenced by natural phenomena (i.e. dryness of Hamoun lakes, land use land cover changes, soil

moisture, frequency and intensity of dust storms) and meteorological conditions, i.e. wind speed and direction, variability in precipitation, etc.

**Table 6.2:** Coefficient of determination ($R^2$) values from the correlations between the monthly values of the multiple satellite sensors over Sistan region. *[N: number of data; a.: lack of common period for the correlations; **: The correlation is significant at the 0.05 level]*

| | | Earth Probe | OMI | MISR | Terra MODIS | Aqua MODIS |
|---|---|---|---|---|---|---|
| **Earth Probe** | Correlation | 1 | | | | |
| | N | 65 | | | | |
| **OMI** | Correlation | a. | 1 | | | |
| | N | 0 | 84 | | | |
| **MISR** | Correlation | 0.839** | 0.819** | 1 | | |
| | N | 22 | 72 | 130 | | |
| **Terra MODIS** | Correlation | 0.654** | 0.783** | 0.791** | 1 | |
| | N | 22 | 36 | 94 | 94 | |
| **Aqua MODIS** | Correlation | a. | 0.763** | 0.790** | 0.963** | 1 |
| | N | 0 | 84 | 102 | 66 | 114 |

The data series of the aerosol properties from the different sensors reveal different trends over the time period of each sensor. More specifically, Nimbus 7 and Earth Probe AI values show an increasing trend for the periods 1979 to 1992 and 1997 to 2001, respectively, which is statistically significant for Earth Probe (+29.65%). These trends are strongly controlled by the considerable increase in aerosol loading during early 2000s following the extreme droughts after 1999 that modified the Land Use Land Cover (LULC) conditions over Hamoun Basin causing the dryness of the lakes. With the exception of the three shallow freshwater lakes (see Fig. 2.4), the wetlands dried completely, leaving deposits of alluvial silt, which is easily lifted by the wind. As a consequence, the dust erosion becomes easier causing more frequent and massive dust storms, especially during summer when the Levar winds are more intense.

Several previous studies (see Engelstaedter *et al*., 2006, and references therein) have shown an association between dust erosion, source regions and intensity in dust storms with rainfall amount over the desert areas. Such an association was also examined over Sistan region by using the rainfall data from the Zabol meteorological station during the period 1979 to 2011*(http://www.irimo.ir/english/province/systan.asp*). In general, the results reveal an inverse relationship between aerosol loading and precipitation (Fig. 6.3)

over Sistan, since the periods with increased precipitation are associated with lower AOD and AI and vice versa. More specifically, during 1979 to 1981 the precipitation was higher and associated with lower AI values compared to the flowing years; AI is relatively high between 1985-1990 due to decrease in precipitation. The most characteristic period is after 1999 when the lowest precipitation amounts and the highest values for both AOD and AI are shown.

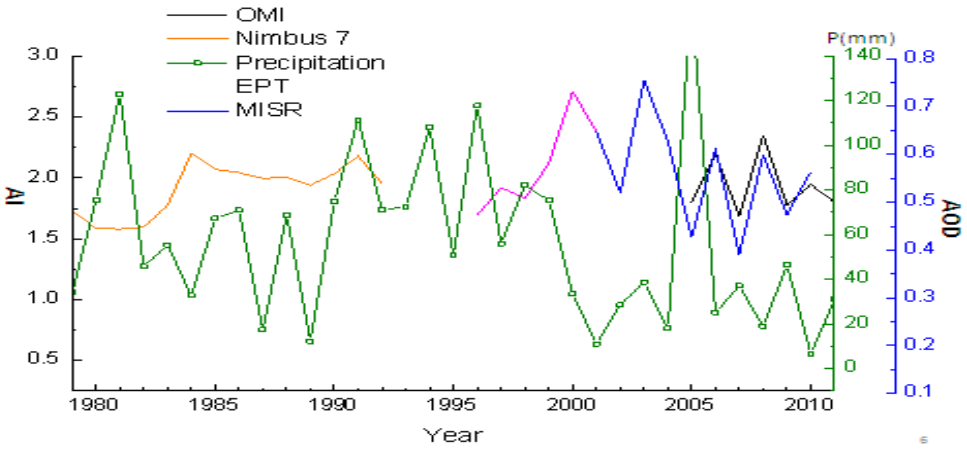


**Figure 6.3:** Annual average of Aerosol Index (AI) and aerosol optical depth (AOD) with annual average of precipitation at the Zabol meteorological station during 1979 to 2011.

Especially in 2001, the accumulated rainfall over Zabol was 11 mm against the annual average of 55 mm. This resulted in late spring and summer seasons of 2001, increasing the EP-AI to ~2.6, the MISR-AOD to 0.6-0.7 and the Terra-MODIS AOD to 1.5-1.9 in June-July of 2001. On the other hand, the abnormal precipitation (~130 mm) in 2005 (Fig. 6.4) has a direct signal in the low AOD values during this year (Fig. 6.3). The multi-year variation of the precipitation amount over Zabol on both annual and monthly basis during the period 1979 to 2011 is shown in Fig. 6.4. In general, the results establish a close relation between aerosol loading and precipitation over Sistan. Thus, the soil moisture and the amount of water surface in Hamoun lakes affect the frequency and intensity of dust storms, similarly to that found over Thar desert, where the amount of suspended aerosols was very different between two contrasting monsoon years (Gautam *et al.*, 2009b). However, it should be noted that the water surface in Hamoun lakes depends on several other factors including temperature, number of rainy days, and rainfall amounts in Afghanistan from where rivers and tributes bring water to Hamoun lakes. In the recent

years, due to saving of water in two reservoir dams (Arghandab dam and Kajaki dam), the volume of water to Hamoun Basin has been significantly reduced, while the regression analysis showed a pronounced declining trend in precipitation of ~-1 mm/yr or -58.4% during the period 1979-2011 over Zabol.

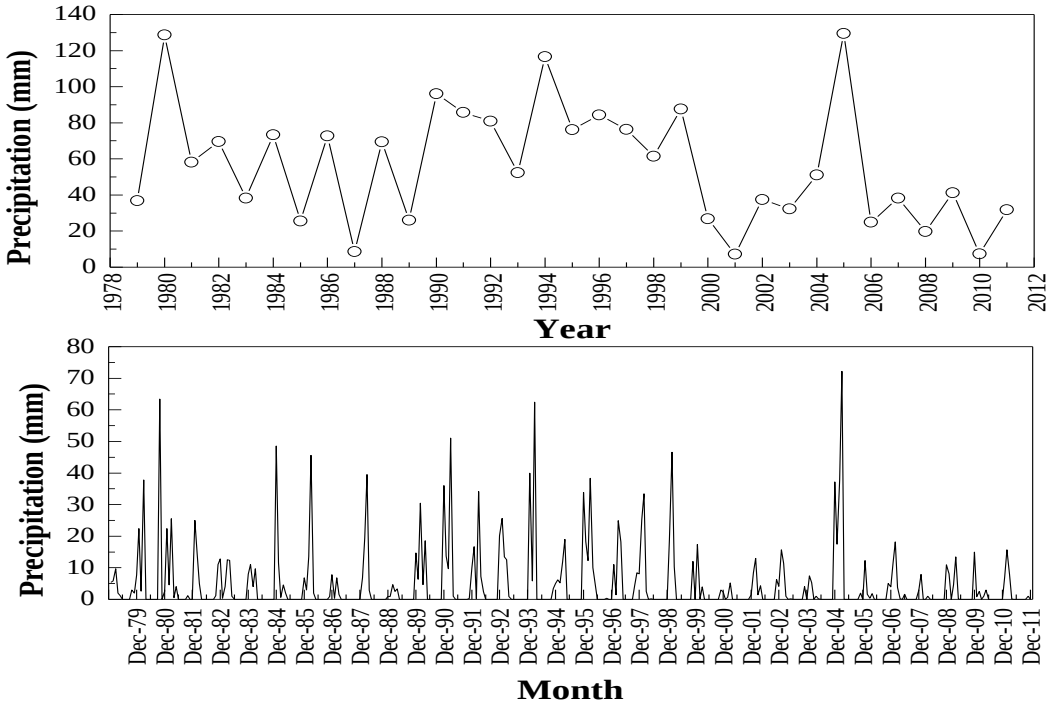


**Figure 6.4:** Multi-year variation of the annual accumulated rainfall values at the Zabol meteorological station during 1979 to 2011.

The annual mean variation of the OMI and AOD values from the various sensors is shown in a common diagram in Fig. 6.5. All sensors agree to a clear-defined annual variation of summer maximum and winter minimum values, without any significant discrepancies from this pattern. This pattern is similar to those found over sites in the Arabian Peninsula and Persian Gulf (Smirnov *et al.*, 2002; Kambezidis and Kaskaoutis 2008; Kim *et al.*, 2011) as well as over the Thar desert (Dey and di Girolamo, 2010), indicating maximum aerosol loading during the summer season due to more frequent and intense dust events, longer aerosol lifetime and absence of precipitation. The AODs from MISR and Aqua MODIS seem to be similar during the months September to February, while MISR underestimates MODIS during the rest of the year. On the other hand, Terra-MODIS exhibits significantly higher AODs from May to August due to the extreme AODs of these months in 2001 (Fig. 6.5). For the same reason, the EP-AI values are much higher than those of Nimbus 7 and OMI during this period (May to August).

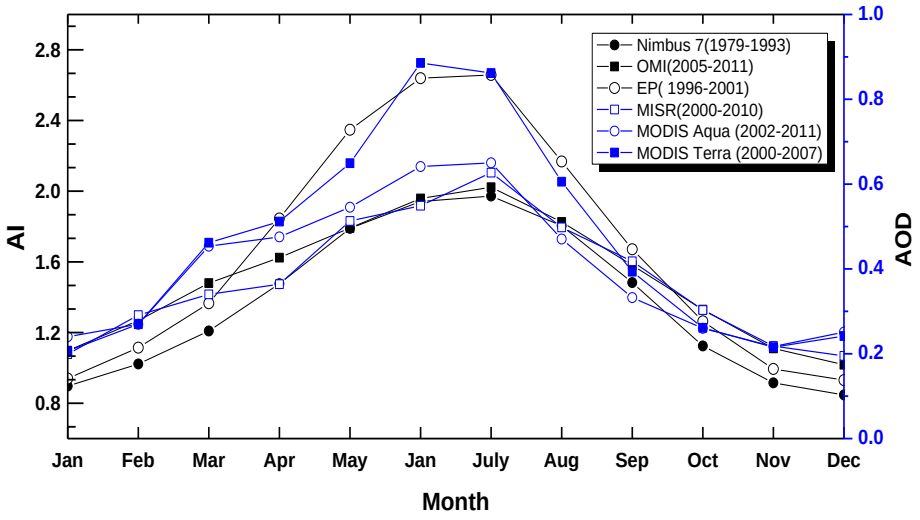


**Figure 6.5:** Annual mean variation of AOD and AI for different satellite sensors and time periods over Sistan region.

The mean, median as well as the distribution of AI and AOD values from the different sensors are presented in a common diagram (Fig. 6.6) in box charts view (see Figure caption for details). Concerning AI, Earth Probe exhibits the higher mean value and standard deviation (1.55±0.54) compared to Nimbus 7 (1.36±0.44) and OMI (1.51±0.38) due to AI peaks in 2001, a period that does not exist in Nimbus 7 and OMI data sets. These values of AI are lower than those reported over the Sahara (Alpert *et al*., 2004; Engelstaedter et al., 2006), but similar to those found over the Thar desert (Gautam *et al*., 2009b, c). On the other hand, MISR AOD (0.38±0.16) is similar to that of Aqua MODIS (0.39±0.20), although different procedures and algorithms are used for the aerosol retrievals over land from the two sensors (Chin *et al*., 2006; Kahn *et al*., 2010). However, due to the enhanced 2001 values, Terra MODIS exhibits higher AOD over Sistan (0.47±0.32). This much higher value is also influenced by the lower time period of Terra-MODIS Deep Blue retrievals (2000-2007) compared to the other sensors.

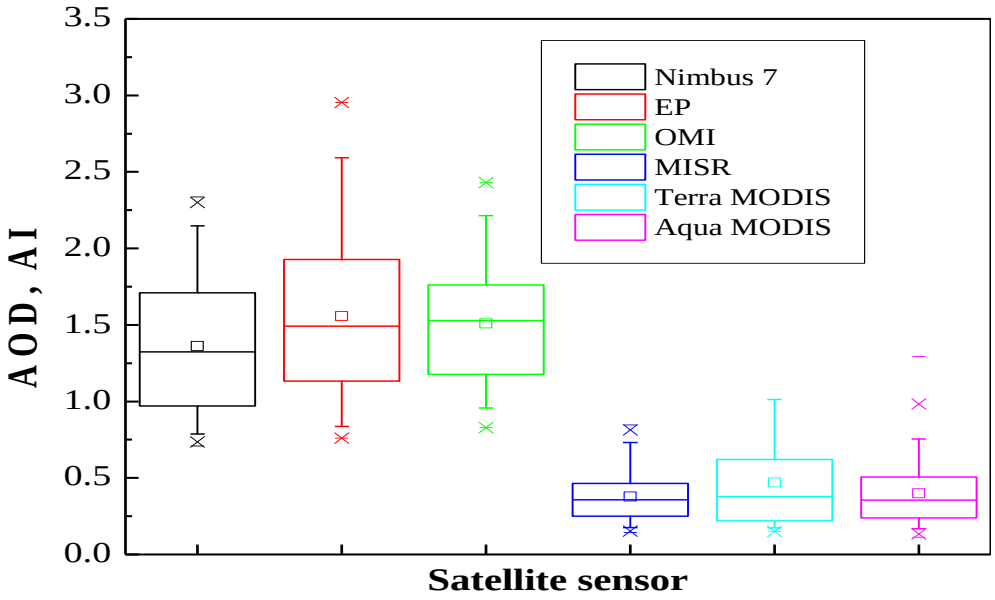


**Figure 6.6:** Box charts view of the Aerosol Index (AI) and Aerosol Optical Depth (AOD) values for different satellite sensors over Sistan region. Each box contains 50% of the values (25% to 75%). The line is the median and the small square the mean value. The standard deviations are defined by the vertical bars, while 1% and 99% of the data donate by the symbol∗; the maximum and minimum values are defined by the symbol - .

Since the aerosol loading exhibits a pronounced seasonal variability over Sistan as shown in Fig. 6.5, the multi-year variability of AI and AOD is also analyzed on a seasonal basis (Fig. 6.7). Winter exhibits the lowest values of both AI and AOD without any significant yearly variation, except the declining trend observed by EP-AI. In spring, the AI and AOD values start to increase, with the Nimbus 7 AI showing an increasing trend, while the maximum AI is shown for EP during 2000 to 2001. The AOD values during 2000s exhibit a rather neutral or even slight decreasing trend for all sensors indicating a decrease in dust-aerosol loading or even dust activity over Sistan region, as also found over northern India via MISR (Dey and di Girolamo, 2011) and MODIS (Kaskaoutis *et al.*, 2011) observations as well as over south Asia via GOCART simulations (Kaskaoutis *et al.*, 2011). Both AOD and AI values increase further in summer, when the multi-year variability and trends are similar to those found in spring, but are even more intense, i.e. increasing for Nimbus 7 and EP and decreasing for the other sensors. In autumn, the AI and AOD values are significantly reduced and the pattern seems to be similar to that observed in winter.

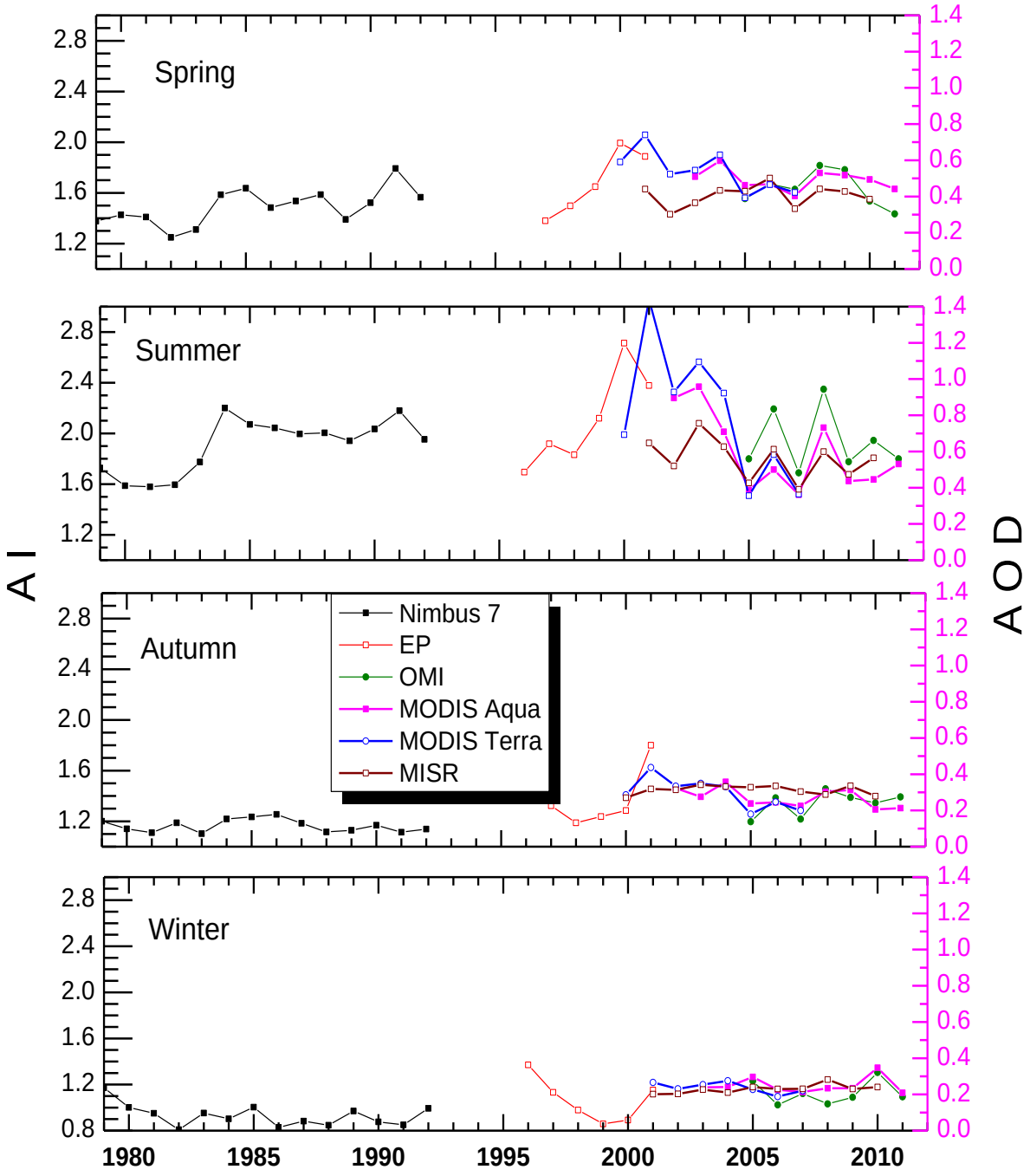


**Figure 6.7:** Multi-year seasonal variation of Aerosol Index (AI) and Aerosol Optical depth (AOD) values from different sensors over the Sistan region.

The monthly and seasonal mean values of AI and AOD from multiple satellite sensors over Sistan region (Latitude, Longitude) during different time periods are summarized in Tables 6.3, 6.4 and 6.5.

**Table 6.3:** Monthly and seasonal variability of Nimbus 7 TOMS (N7T), Earth Probe TOMS (EP), OMI AI and MISR AOD over the Sistan region.

| | Nimbus 7 | EP | OMI | MISR |
|---|---|---|---|---|
| **January** | 0.897 | 0.940 | 1.097 | 0.199 |
| **February** | 1.022 | 1.115 | 1.268 | 0.291 |
| **March** | 1.209 | 1.366 | 1.480 | 0.340 |
| **April** | 1.476 | 1.845 | 1.624 | 0.364 |
| **May** | 1.789 | 2.347 | 1.792 | 0.513 |
| **June** | 1.942 | 2.639 | 1.959 | 0.549 |
| **July** | 1.972 | 2.658 | 2.022 | 0.627 |
| **August** | 1.804 | 2.168 | 1.826 | 0.498 |
| **September** | 1.483 | 1.671 | 1.580 | 0.418 |
| **October** | 1.124 | 1.263 | 1.330 | 0.303 |
| **November** | 0.915 | 0.994 | 1.110 | 0.218 |
| **December** | 0.847 | 0.931 | 1.018 | 0.195 |
| **Spring** | 1.555 | 1.670 | 1.628 | 1.816 |
| **Summer** | 1.799 | 2.193 | 1.689 | 2.349 |
| **Autumn** | 1.197 | 1.384 | 1.218 | 1.456 |
| **Winter** | 1.230 | 1.023 | 1.122 | 1.032 |
| **Annual** | **1.445** | **1.568** | **1.414** | **1.663** |

**Table 6.4:** $AOD_{550}$ over Sistan region based on Terra-MODIS Deep Blue retrievals during the period 2000-2007.

| **Year** | **2000** | **2001** | **2002** | **2003** | **2004** | **2005** | **2006** | **2007** | **annual** |
|---|---|---|---|---|---|---|---|---|---|
| **Month** | | | | | | | | | |
| **Jan** | | 0.22 | 0.229 | 0.2 | 0.16 | 0.16 | 0.193 | 0.284 | 0.207 |
| **Feb** | | 0.397 | 0.245 | 0.276 | 0.306 | 0.285 | 0.176 | 0.202 | 0.270 |
| **Mar** | 0.811 | 0.392 | 0.368 | 0.457 | 0.621 | 0.319 | 0.301 | 0.425 | 0.462 |
| **Apr** | 0.37 | 0.708 | 0.521 | 0.521 | 0.738 | 0.45 | 0.386 | 0.4 | 0.512 |
| **May** | 0.645 | 1.12 | 0.681 | 0.658 | 0.531 | 0.409 | 0.709 | 0.441 | 0.649 |
| **Jun** | 0.688 | 1.979 | 0.85 | 0.975 | 0.939 | 0.472 | 0.519 | 0.466 | 0.886 |
| **Jul** | 0.747 | 1.52 | 1.006 | 1.296 | 0.96 | 0.379 | 0.782 | 0.379 | 0.862 |
| **Aug** | 0.307 | 0.816 | 0.929 | 1.013 | 0.868 | 0.217 | 0.447 | 0.248 | 0.606 |
| **Sep** | 0.345 | 0.469 | 0.547 | 0.518 | 0.474 | 0.203 | 0.372 | 0.22 | 0.394 |
| **Oct** | 0.205 | 0.482 | 0.305 | 0.234 | 0.315 | 0.174 | 0.187 | 0.188 | 0.261 |
| **Nov** | 0.181 | 0.36 | 0.15 | 0.296 | 0.204 | 0.162 | 0.181 | 0.19 | 0.215 |
| **Dec** | | 0.219 | 0.287 | 0.361 | 0.238 | 0.196 | 0.176 | 0.215 | 0.242 |
| **Winter** | 0.194 | 0.160 | 0.210 | 0.187 | 0.140 | 0.105 | 0.116 | 0.079 | 0.149 |
| **Spring** | 0.275 | 0.383 | 0.338 | 0.373 | 0.415 | 0.146 | 0.204 | 0.194 | 0.291 |
| **Summer** | 0.256 | 0.434 | 0.479 | 0.518 | 0.402 | 0.106 | 0.251 | 0.134 | 0.323 |
| **Autumn** | 0.122 | 0.245 | 0.192 | 0.189 | 0.188 | 0.065 | 0.123 | 0.074 | 0.150 |

**Table 6.5:** $AOD_{550}$ over Sistan region based on Aqua-MODIS Deep Blue retrievals during the period 2002 to 2011.

| Year | 2002 | 2003 | 2004 | 2005 | 2006 | 2007 | 2008 | 2009 | 2010 | 2011 | Annual |
|---|---|---|---|---|---|---|---|---|---|---|---|
| Month | | | | | | | | | | | |
| Jan | | 0.209 | 0.149 | 0.216 | 0.214 | 0.279 | 0.162 | 0.222 | 0.523 | 0.187 | 0.240 |
| Feb | | 0.254 | 0.229 | 0.345 | 0.241 | 0.177 | 0.297 | 0.347 | 0.342 | 0.194 | 0.270 |
| Mar | | 0.455 | 0.647 | 0.369 | 0.348 | 0.378 | 0.5 | 0.493 | 0.534 | 0.359 | 0.454 |
| Apr | | 0.465 | 0.644 | 0.534 | 0.392 | 0.39 | 0.441 | 0.504 | 0.529 | 0.381 | 0.476 |
| May | | 0.609 | 0.501 | 0.483 | 0.665 | 0.442 | 0.649 | 0.557 | 0.42 | 0.584 | 0.546 |
| Jun | | 0.871 | 0.755 | 0.515 | 0.465 | 0.505 | 0.984 | 0.512 | 0.468 | 0.698 | 0.641 |
| Jul | 0.842 | 1.294 | 0.671 | 0.393 | 0.714 | 0.361 | 0.692 | 0.445 | 0.552 | 0.537 | 0.650 |
| Aug | 0.955 | 0.709 | 0.7 | 0.256 | 0.321 | 0.218 | 0.519 | 0.353 | 0.317 | 0.357 | 0.471 |
| Sep | 0.506 | 0.381 | 0.445 | 0.259 | 0.315 | 0.229 | 0.41 | 0.32 | 0.267 | 0.191 | 0.332 |
| Oct | 0.309 | 0.201 | 0.368 | 0.234 | 0.25 | 0.217 | 0.277 | 0.298 | 0.237 | 0.209 | 0.260 |
| Nov | 0.153 | 0.245 | 0.261 | 0.221 | 0.169 | 0.228 | 0.223 | 0.321 | 0.112 | 0.238 | 0.217 |
| Dec | 0.253 | 0.346 | 0.328 | 0.222 | 0.184 | 0.244 | 0.134 | 0.177 | 0.246 | 0.376 | 0.251 |
| Winter | | 0.239 | 0.241 | 0.296 | 0.226 | 0.213 | 0.234 | 0.234 | 0.347 | 0.209 | 0.249 |
| Spring | | 0.510 | 0.597 | 0.462 | 0.468 | 0.403 | 0.530 | 0.518 | 0.494 | 0.441 | 0.492 |
| Summer | 0.895 | 0.958 | 0.709 | 0.388 | 0.500 | 0.361 | 0.732 | 0.437 | 0.446 | 0.531 | 0.596 |
| Autumn | 0.323 | 0.276 | 0.358 | 0.238 | 0.245 | 0.225 | 0.303 | 0.313 | 0.205 | 0.213 | 0.270 |

## 6.4. Spatial distribution of aerosols over southwest Asia and Sistan

In this section the spatial distribution of aerosols over southwest Asia, in general, and Sistan region, in particular, is analyzed on seasonal basis by means of different satellite sensors in order to compute and compare the annual aerosol cycle over a wide area surrounding Sistan. Figure 6.11 summarizes the spatial distribution maps of the seasonally averaged values of AI from Nimbus 7 and OMI and of AOD values from MISR and Aqua MODIS. Both variables (AI and AOD) present a pronounced seasonal variability over southwest Asia with winter minima and summer maxima similar to that found for the Sistan region (Fig. 6.8). As far as the AI is concerned the results exhibit similar spatial distribution for Nimbus 7 and OMI over the whole area and for each season. More specifically, during spring the hot-spot AI areas are defined in the Sistan region and Hamoun Basin, eastern Pakistan and in the Arabian Peninsula without influencing significantly the Arabian Sea. During summer the AI values are higher over the whole area compared to those in spring with the most important increases to be defined over the major dust sources in southwest Asia, i.e. Hamoun Basin, eastern Pakistan and southeastern Arabian Peninsula. In this season significant amount of UV-absorbing aerosols at higher altitudes corresponding to dust, mainly originated from Arabian Peninsula, is transported

over the Arabian Sea from westerlies at higher altitudes (>700 hPa) as shown in Lawrence and Lelieveld (2010). Furthermore, the northernmost part of Arabian Sea is also strongly influenced by the dust storms that originated from the Hamoun Basin and the arid areas of Iran, Pakistan and Afghanistan since the Arabian Sea is in the downwind direction of the Levar winds. By the end of summer the dust activity over the region is significantly reduced as well as the dust-aerosol lifetime in the atmosphere due to increased precipitation mainly over the oceanic areas. However, over land, some limited areas of increased AI still exist (autumn and winter), such as Hamoun Basin and southern Afghanistan and some areas in the Arabian Peninsula. The increased AI observed in autumn over northeastern Pakistan corresponds mainly to biomass burning aerosols, and not to dust, since this is the season of crop-residue burning over the Punjab (Badarinath *et al*., 2009; Sharma et al., 2010).

The AOD spatial distributions both from MISR and Aqua MODIS are rather similar to each other and with those observed for AI. However, the deep blue algorithm over land applied to Aqua MODIS observations overestimates the AOD compared to MISR at least over hot spot areas or over the dust source regions as shown for Sistan and eastern Pakistan for spring and summer. This inconsistency is mainly attributed to the different algorithm and procedures used for aerosol retrievals from the two sensors as well as to the fact that MODIS provides nearly daily observations over the area, while MISR one per week, approximately. Thus, some intense dust storms, mainly in summer, may not be detected by MISR, thus the lower AODs over the dust source regions and downwind areas. Note also that the sampling period is different for the two sensors, i.e. 2000 t0 2010 for MISR and 2002 to 2011 for Aqua-MODIS. In contrast, MISR exhibits higher values in autumn and winter over the arid regions of Arabian Peninsula, while both sensors highlight the enhanced AOD over northeastern Pakistan during late autumn and winter caused by smoke aerosols from crop residue burning over the area.

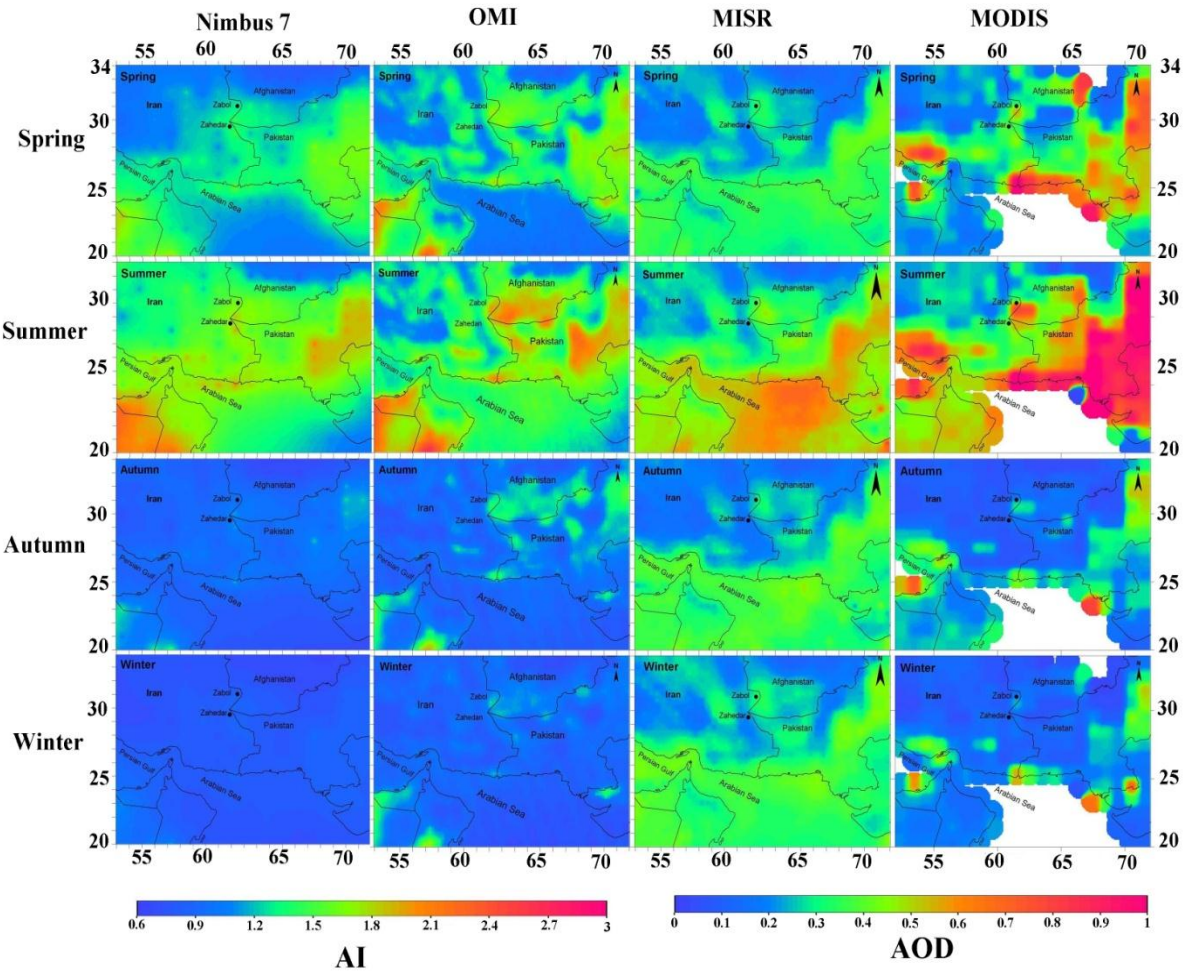


**Figure 6.8:** Seasonal maps of the spatial distribution of AI (Nimbus 7 and OMI) and AOD (MISR and MODIS) values over southwest Asia. The period of measurements are: for Nimbus 7 (1979 to 1992), for OMI (2005 to 2011), for MISR (2000 to 2010) and for Aqua-MODIS (2002 to 2011).

The use of TOMS and OMI AI satellite data presents some promising results for the identification of dust source regions, although they have a larger spatial resolution compared to MODIS (Baddock *et al*., 2009). Therefore, the use of OMI-AI satellite data for the identification of major dust sources over southwest Asia allows one to focus on critical regions and to characterize emission rates in response to environmental conditions. Apart from the seasonal spatial distribution of AI (Fig. 6.8), the OMI-AI over southwest Asia bounded from 20 to 34$^{o}$N and 52 to 72$^{o}$E is also examined on monthly basis during the period 2005 to 2011 (Fig. 6.9). The AI concern data via the Aura-OMI Level-2G (Version 003) with a spatial resolution of 0.25$^{o}$ x 0.25$^{o}$ obtained from Giovanni.

The spatial distribution of AI values reveals a considerable annual variation in aerosol load, in general, and in dust occurrence, in particular. During the winter season (December to February) the AI is generally low, except for some hotspot regions with values of above 1.5, e.g. Hamoun Basin. From March onwards high AI values start to spread over a wider area, covering southern Afghanistan (near to Hamoun), as well as the Arabian and Thar deserts. The AI continuously increases until May, with the highest increase over the Thar desert influencing the aerosol load in northern India (Gautam *et al.*, 2009; Dey and di Girolamo, 2010). During the summer period (June to August) the AI significantly increases over the northern Arabian Sea due to the large influence of dust coming from Arabia as well as from Iran and Pakistan due to strong northern Levar winds. This is also the period with the highest AI over Sistan which is closely associated with a reduction in visibility and stronger winds. From September to November the high AI is limited over Sistan, as well as over some hotspots in Arabia and northeastern Pakistan. From the AI spatial distribution one may put emphasis on the large regional differences between Zabol (near to Hamoun basin) and the city of Zahedan, located about 200 km south. The AI at Zabol is significantly higher during all months, suggesting a larger presence of dust compared to the adjacent southern areas. This is consistent with the large differences in $PM_{10}$ concentrations found between Zabol and Zahedan (See chapter 4).

In synopsis, the spatial distribution of AI identified the Hamoun basin as one of the most active dust source regions in southwest Asia. In general, the dust sources, regardless of size or wind strength, are usually associated with topographic lows in close proximity to mountains and highlands with annual rainfall of less than 200 to 250 mm (Prospero *et al.*, 2002; Engelstaedter *et al.*, 2006). The topography and meteorological conditions in Hamoun favor such a dust outflow. As mentioned in the previous Chapters, this region is associated with drainage features and extensive alluvial deposits, exhibiting some similarities with the lowlands south of the Atlas Mountains in northwest Sahara (Kahn *et al.*, 2009) and Lake Eyre in Australia (Baddock *et al.*, 2009). The accumulation of recent and ancient sediments in such areas, often with salt, which enhances the weathering of sediments, makes them good sources of fine-grained mineral particles (Middleton, 1986) which might be transported potentially thousands of kilometers downwind.

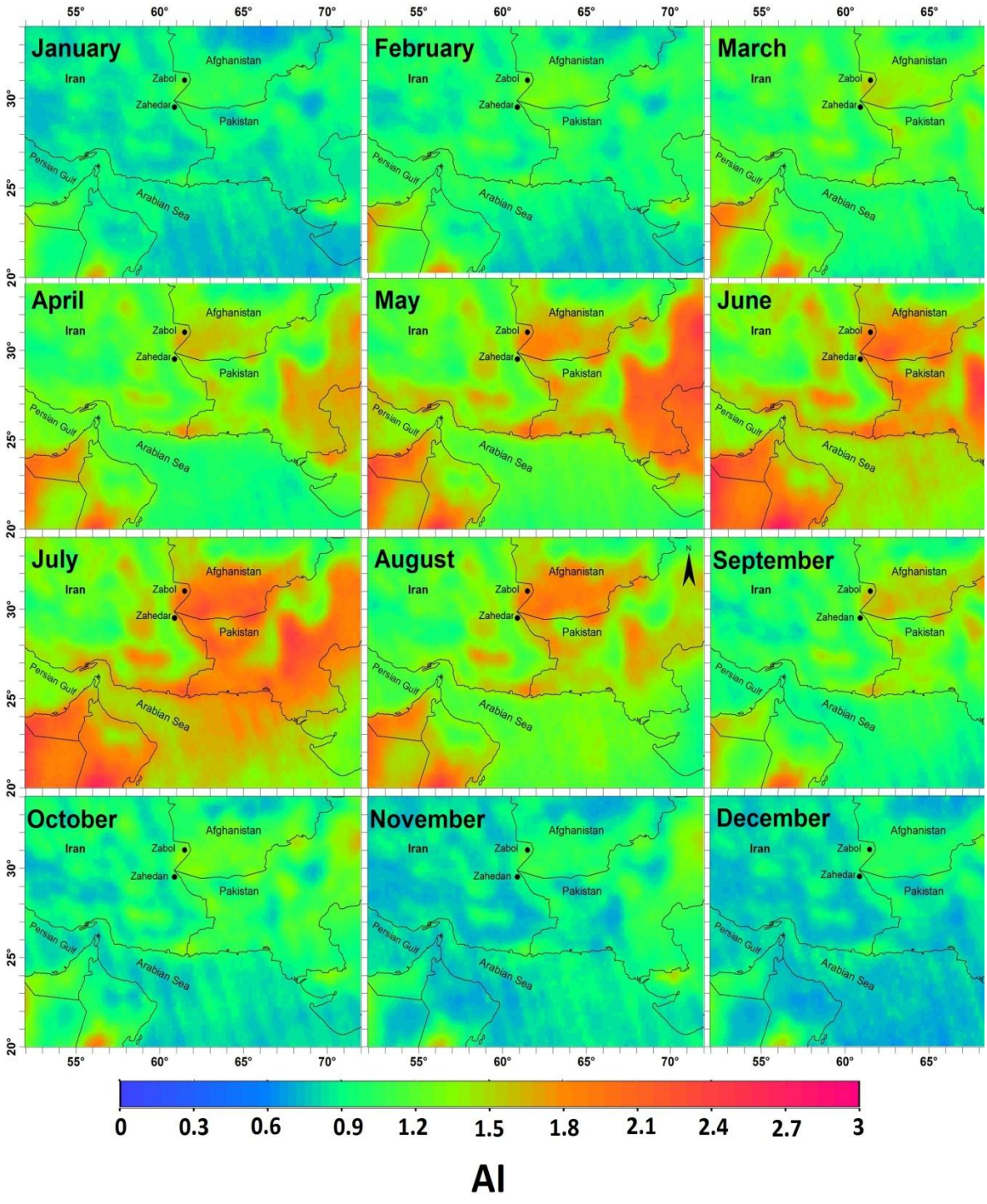


**Figure 6.9:** Monthly mean spatial distribution of Ozone Monitoring Instruments (OMI) satellite observations over southwest Asia during the period 2005 to 2011.

Intense dust storms originated from Hamoun are responsible for the dramatic increase in AOD over the downwind areas. Alam et al. (2011) reported that such an intense dust plume , which occurred on 21 July 2007 affected coastal AS to such an extent that the AOD increased in Karachi to 1.36. The monthly mean spatial AOD variation via MISR (2000-2010) over southwest Asia is shown in Fig. 6.10. The AOD monthly mean spatial distribution over southwest Asia is similar to that observed for OMI-AI for the reasons discussed above. Once again, the AOD values increase considerably in late spring and summer months, especially in Hamoun, eastern Pakistan, Arabia and Arabian Sea. On the other hand, during winter months high AOD values are observed only over the Indus basin in Pakistan and in some areas in the Arabian Peninsula and Sistan. The former is attributed mainly to anthropogenic aerosols during this period over the densely populated Indus Basin and not to dust presence, since dust activity is low during the winter season in southwest Asia (note the very low AOD values over nearly the whole Iran and Afghanistan during the period November to February suggesting absence of anthropogenic aerosols and very low dust activity).

Finally, the AOD spatial distribution from Aqua MODIS deep blue algorithm over land during the period 2002 to 2010 is shown in Fig. 6.11. In these graphs the ocean pixels have been removed as the aerosol retrievals over sea are obtained with a different algorithm. Also, larger uncertainties in the AOD retrievals exist in the coastal areas due to ocean-land sub-pixel contamination. For this reason there are pockets of very high AODs near to coastal areas which seem to be unreal taking into account the neighboring pixels. Furthermore, the Sistan region is defined in the graph as the annual AOD variation (see section 6.3) and the AOD trends (see next section) are examined in more detail over this area.

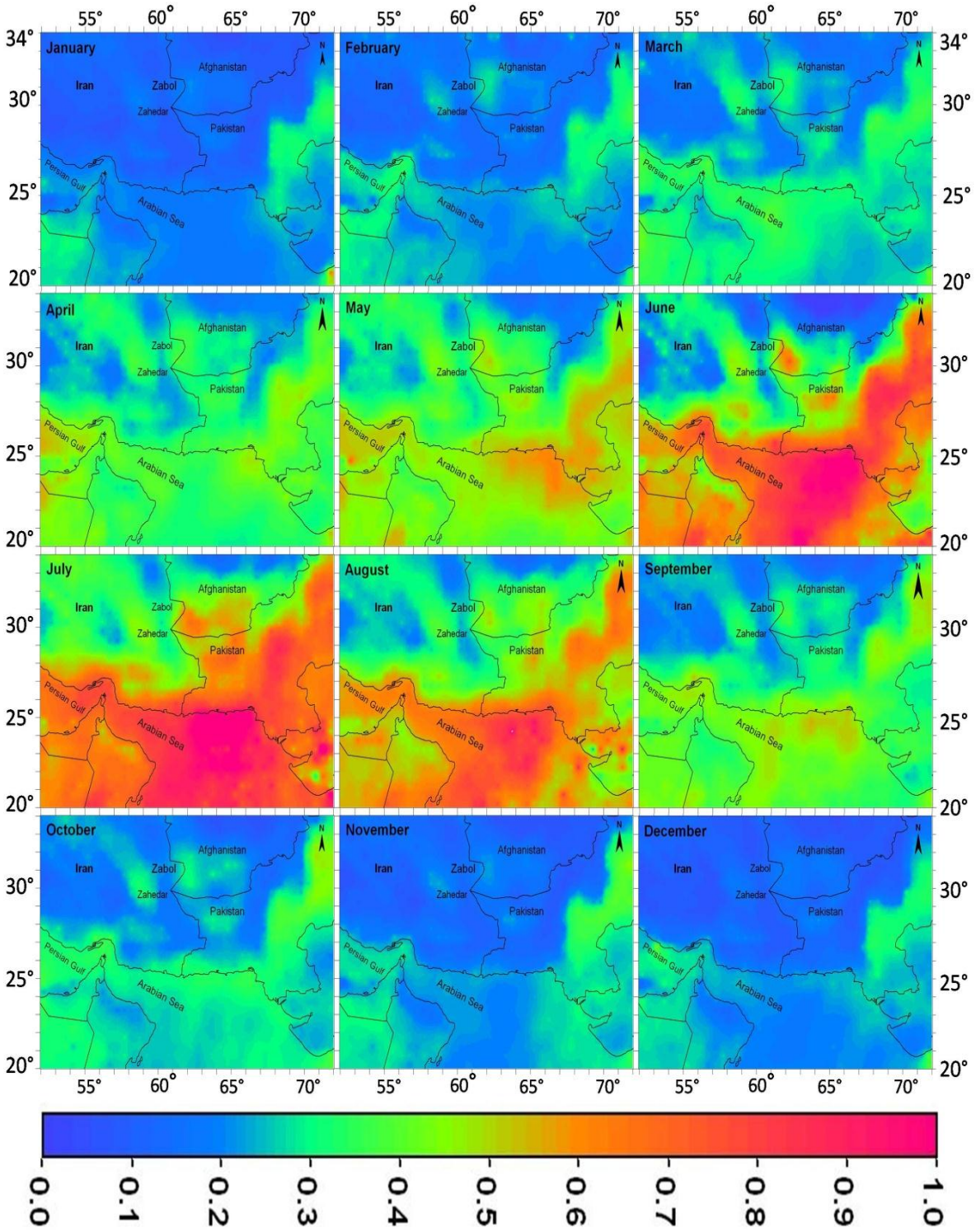


**Figure 6.10:** Monthly mean spatial distribution of MISR Aerosol Index (AOD) over southwest Asia during the period 2000 to 2010.

Fig. 6.11 reveals a similar spatial and monthly distribution of AOD over southwest Asia from Aqua-MODIS as that found from MISR over the same region (Fig. 6.10). So, any new discussion about the annual variation of the AOD spatial distribution and the reason influencing it is avoided. It is characteristic that both Aqua MODIS and MISR exhibit similar values over Sistan region as also shown in Fig. 6.5.

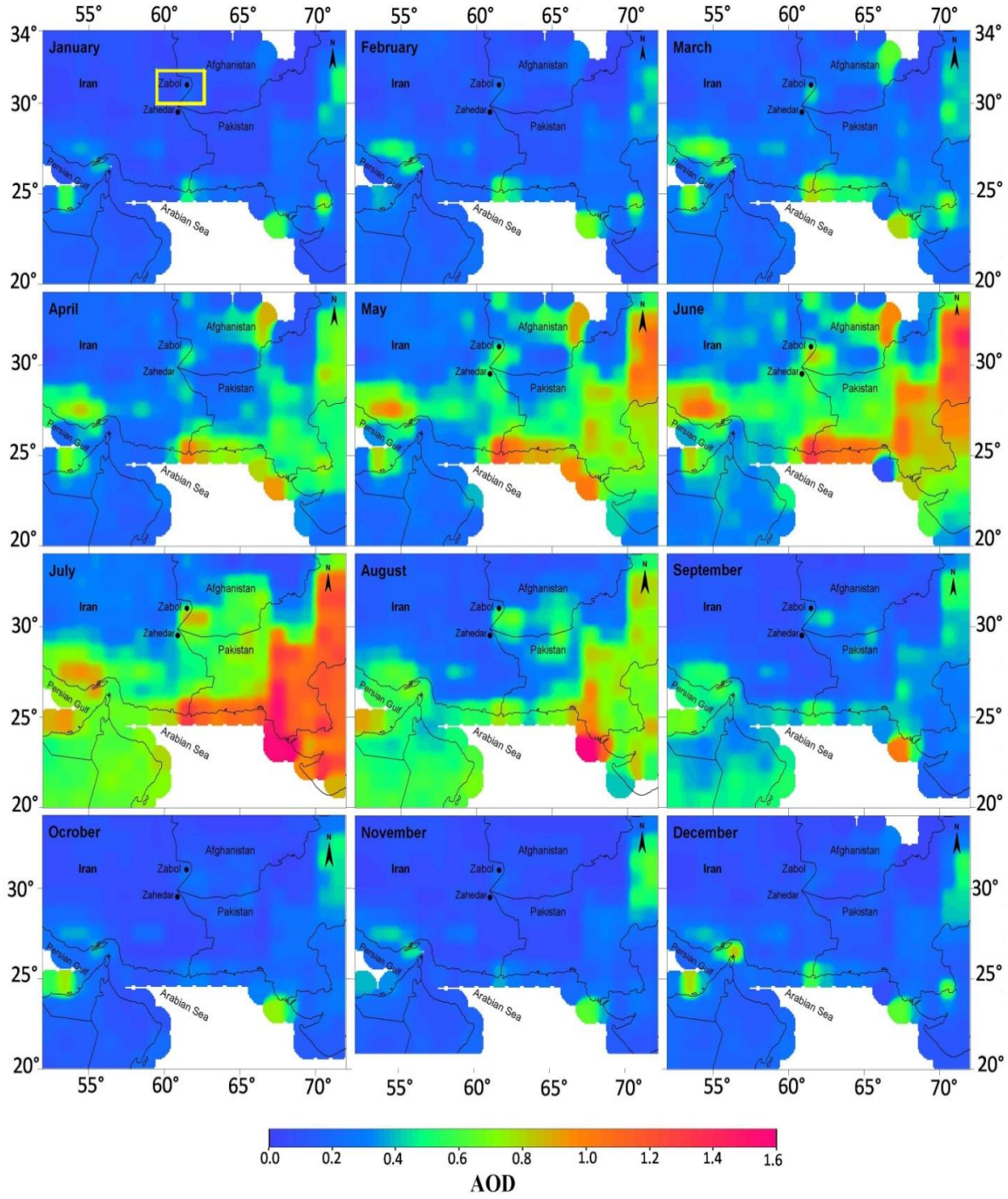


**Figure 6.11:** Monthly mean spatial distribution of Aqua MODIS satellite observations over southwest Asia during 2000 to 2010.

### 6.5 Aerosol trends over southwest Asia detected from satellites

Recently, the investigation of the aerosol trends over an extended area via satellite remote sensing has created great scientific interest with respect to the view of the accuracy of the computed trends as compared to aerosol trends obtained from AERONET stations (Prasad and Singh, 2007; Dey and di Girolamo, 2011; Kharol *et al*., 2011). On the other hand, the large spatial coverage of the satellite sensors and ad up to ten years of recordings establish them as a useful tool for the monitoring of the aerosol trends from space (Mishchenko *et al*., 2009; Zhang and Reid, 2010; Kaskaoutis *et al*., 2011). Southwest Asia, as shown in this Chapter, has not received a great attention from satellite remote sensing or ground-based instrumentation such as the neighboring Indian subcontinent and adjoining oceanic regions. With the increase in population, urbanization, industrialization and demands for energy, the aerosol load over south Asia is gradually increasing and having a significant impact on the continuation of solar dimming (Ohmura, 2009; Badarinath *et al*., 2010). The increasing aerosol emissions, mainly from anthropogenic activities, are responsible for the presence of the atmospheric brown clouds (Ramanathan *et al*., 2007), which have significant climate implications in view of heating of the middle and upper troposphere (Gautam *et al*., 2010). However, the arid environments of southwest Asia are sparsely populated without any significant industrial and anthropogenic activity except for the Indus basin in Pakistan. Thus, the spatial distribution and trends of aerosols over this region are mainly affected by the natural variability of aerosols and dust activity.

Fig. 6.15 shows, the monthly % variation of the AOD values obtained from MISR during the period 2000-2010. Similar research, i.e. analysis of the MISR AODs trend over Indian sub-continent and adjoining oceanic areas was recently performed by Dey and Di Girolamo (2011). It should be noted that the % AOD variations were estimated via the formula $\Delta AOD = a*N/\overline{AOD}*100$, where a is the slope value computed from the linear regression of the monthly mean values during 2000 to 2010 for each pixel, N the number of years, and $\overline{AOD}$ the mean AOD for each pixel during 2000 to 2010. The results reveal a considerable spatial distribution of the AOD % variations during the last decade, which also exhibits pronounced seasonal and monthly differences. In general, the western part of the study area exhibits positive values corresponding to AOD increasing trends, while the eastern rather neutral or even negative AOD trends during the months February to

October. This declining trend is especially pronounced over the Thar desert and the northeastern part of the Arabian Sea during June to August was also found by Dey and Di Girolamo (2011) using MISR data and Kaskaoutis *et al*. (2011) using MODIS observations. A more recent study over the region (Kaskaoutis *et al*., 2012) has shown that this declining trend is mainly attributed to the extremely large values during these months in years 2002 and 2003 favored by absence of precipitation and longer aerosol lifetime in the atmosphere. This is strong evidence that the AOD trends observed over southwestern Asia, an area without significant anthropogenic emissions and industrial activities, are mainly controlled by the dust annual variability, which in turn is under the influence of the intensity and onset of the monsoon and larger-scale synoptic weather conditions (Gautam et al., 2009). On the other hand, the AOD % variation seems to be positive over Sistan region during the winter period (December to March). However, the calculated trends using the monthly mean AOD values are strongly influenced by the studied period and the intra-annual variation of AOD over a specific area. In cases when month during the beginning or the end of the examining period has extreme low or high AOD value, this value may influence considerably the linear regression trend analysis. Thus, the results of Fig. 6.12 as well as those of Fig. 6.13 corresponding to Aqua MODIS must be considered qualitatively and not quantitatively.

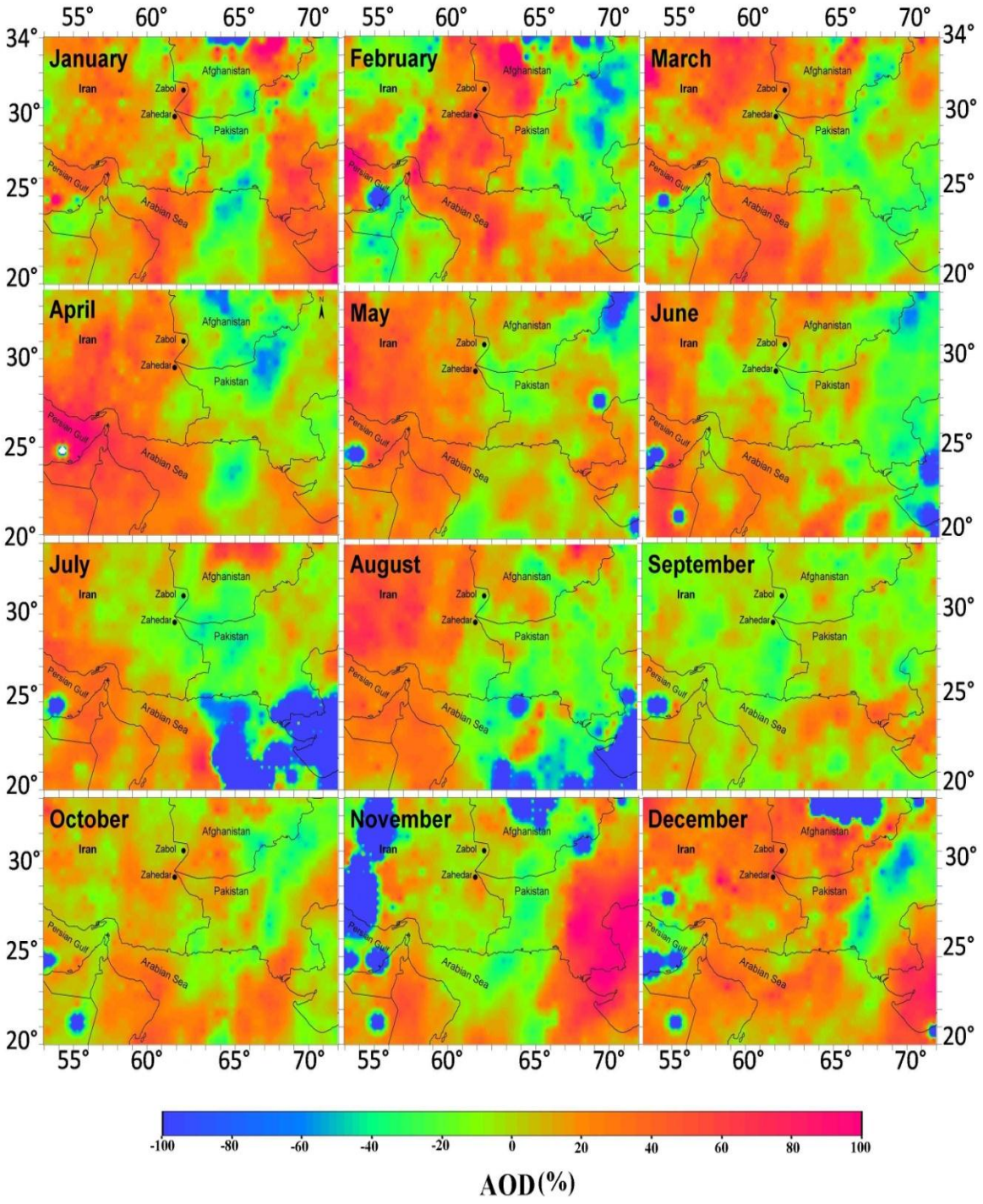


**Figure 6.12:** Spatial distribution of the Aerosol Optical Depth (AOD) % variation obtained from MISR sensor during the period 2000 to 2010 over southwest Asia.

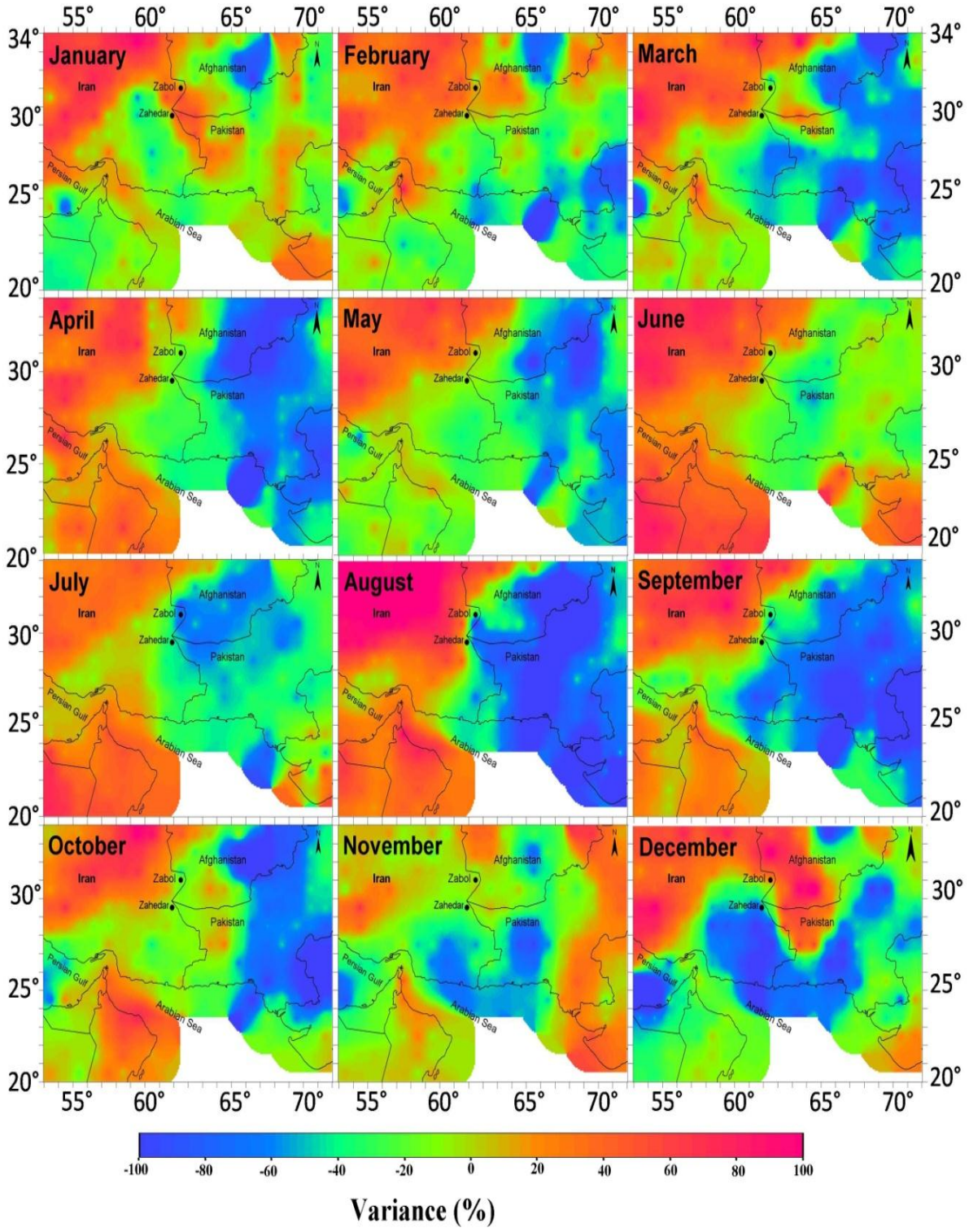


**Figure 6.13:** Spatial distribution of the Aerosol Optical depth (AOD) % variation obtained from Aqua-MODIS sensor (deep blue algorithm) during the period 2000 to 2010 over southwest Asia.

The above statement is justified by comparing the results of the AOD % trends as obtained from the two sensors. In general, the western part of the study area exhibits positive AOD trends for Aqua MODIS as for MISR, and the eastern part negative trends. However, the AOD % variations as well as the spatial distributions exhibit large differences for the two sensors justifying that the length of the study period plays the main role in the AOD trend estimations, which are strongly affected by the intra-annual AOD variation for each month over a specific region (Kaskaoutis *et al*., 2011). Finally, Table 6.6 summarizes the results of the slope values, as obtained from the AOD linear regression analysis, as well as the AOD % variation for both MISR and Aqua-MODIS sensors.

**Table 6.6:** Slope values and % variations of Aerosol Optical depth (AOD) over Sistan region as obtained from MISR and Aqua-MODIS satellite sensors.

| | **Slope MODIS Aqua (2002-2011)** | **Slope MISR (2000-2010)** | **AOD% MODIS Aqua (2002-2011)** | **AOD% MISR (2000-2010)** |
|---|---|---|---|---|
| **Jan** | 0.01657 | 0.00778 | 62.1 | 39.2 |
| **Feb** | 0.00265 | 0.00510 | 8.8 | 17.5 |
| **Mar** | -0.00538 | 0.00907 | -10.7 | 29.3 |
| **Apr** | -0.01153 | 0.00474 | -21.8 | 14.3 |
| **May** | -0.00352 | -0.00698 | -5.8 | -15.0 |
| **Jun** | -0.01733 | -0.00457 | -24.3 | -9.2 |
| **Jul** | -0.05167 | -0.01469 | -79.5 | -25.8 |
| **Aug** | -0.05561 | -0.00770 | -118.2 | -17.0 |
| **Sep** | -0.02358 | -0.00809 | -71.0 | -21.3 |
| **Oct** | -0.00547 | 0.00414 | -21.0 | 15.0 |
| **Nov** | 0.00121 | 0.00290 | 5.6 | 14.6 |
| **Dec** | -0.00443 | 0.00436 | -15.9 | 24.6 |
| **Spring** | -0.00681 | -0.00227 | -12.8 | -3.3 |
| **summer** | -0.04154 | -0.01016 | -74.0 | -21.4 |
| **Autumn** | -0.00928 | 0.00380 | -28.8 | 18.1 |
| **Winter** | 0.00866 | 0.00575 | 18.3 | 27.1 |
| **Annual** | -0.01224 | -0.00033 | -24.3 | -5.2 |

Even though the slope values are of similar magnitude for both sensors in a specific month, the AOD % variations may differ significantly, thus highlighting the significant role of the examined period for such retrievals. Despite the large differences in the monthly % variations, both sensors exhibit a positive trend in AOD (increasing values during the last decade) in winter, except for December as obtained from Aqua-MODIS, and a negative trend (declining in AOD) during late spring and summer months (May to

September). The decreasing in AOD during these months, which are characterized by the higher AOD values and the more frequent and intense dust storms, may suggest a declining trend in the dust activity over Sistan region and Hamoun Basin during more recent years, after the extreme droughts in the beginning of the 2000s. Such a decreasing trend on days with visibility below 2km during recent years has also been shown in Zabol (Fig. 2.11). However, more years must be taken into consideration in order for these mentioned trends to be confirmed. On the other hand, the significant differences revealed by the two sensors require the use of ground-based instrumentation to be compared for such retrievals, which must be compared with satellite sensors in order to stablish the sensors accuracy over this arid environment.

### 6.6. Conclusions

For monitoring dust production and effects of regional-scale atmospheric processes on dust emission and transport over the Sistan, satellite remote sensing data was used to provid observational constraints over the region. The aerosol patterns were analyzed by means of multiple satellite platforms aiming to reveal the spatio-temporal and vertical distribution of dust aerosols. The main focus is to determine similarities and differences in dust climatology provided by these sensors over the Sistan region and surroundings. AI and AOD were used as measures of the atmospheric aerosol load. The analysis used the strength of each data set separately to provide a general picture on how the aerosols vary across different regions of southwest Asia and how this variability relates to the atmospheric environment. The results show a marked seasonal cycle with high aerosol loading during summer and lower in winter, while MISR, MODIS Deep Blue and OMI climatologies agree in both terms of monthly and seasonally mean spatial and temporal AOD patterns revealing similar seasonal behavior over the region. Comparisons of the distribution of the aerosol load between AI and AOD, find similar characteristics in the representation of the main sources of aerosol on Hamoun lakes. Both products are able to represent the maximum values of aerosols, especially for those regions affected by dust aerosols. After prolonged drought conditions in 1999 at Hamoun lakes (northern of Sistan) the dust-aerosol load over the area increased. The higher aerosol concentrations during summer are interpreted as a result of the Levar northerly winds and the drying of Hamoun lakes.